Phy 450 Spring 2021

Lec #9 Electrodynamics of Quarks

<u>In high energy limit</u> $e^+e^- \to q\bar{q}$

$$\sigma_{had} = \frac{\pi}{3}\frac{Q^2}{E^2}\alpha^2$$

Q = quark charge
E = e^+e^- cm beam energy

Then $R(E) = \dfrac{\sigma_{had}}{\sigma_{\mu\mu}} = 3 \sum Q_i^2$ Incoherent sum!

↑ color factor

measured $R(E)$ is strong experimental evidence for quarks and color.

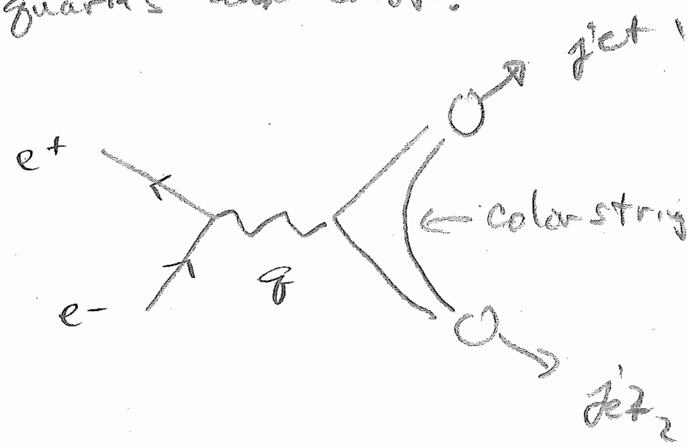

momentum of hadron jets approximates quark momentum

3 jet events are evidence of gluon

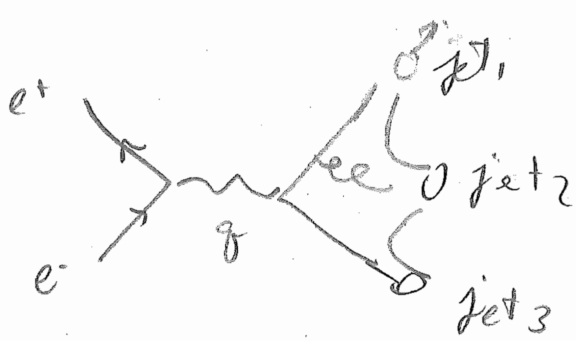

e-p elastic scattering

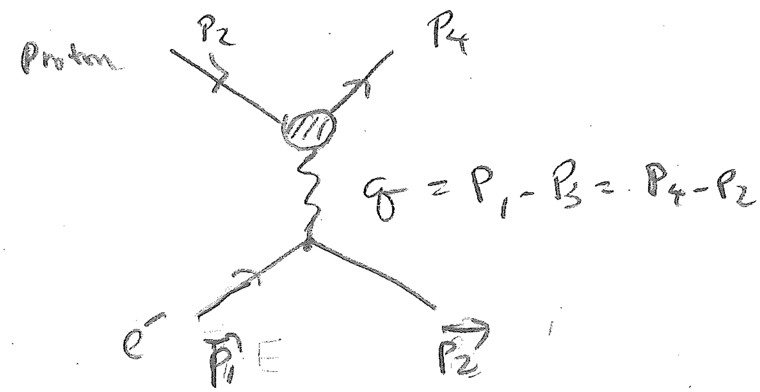

$$\langle |m|^2 \rangle = \frac{1}{4} \sum_{\text{spin}} |m|^2 = \frac{e^4}{q^4} L^{\mu\nu} K_{\mu\nu}$$

spin average

lepton proton

$\frac{1}{2}$ in each factor

$$q^2 = t \Rightarrow -2P_1P_3(1-\cos\vartheta) \quad \text{timelike in general}$$

massless limit

Lab frame
in high energy limit ($m_e \approx 0$)

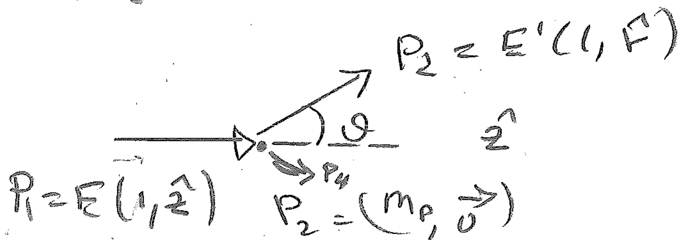

$$\langle |m|^2 \rangle = \frac{e^4}{4EE' \sin^4(\frac{\theta}{2})} \left(2K_1 \sin^2\frac{\vartheta}{2} + K_2 \cos^2 \vartheta/2 \right)$$

$K_1(q^2)$, $K_2(q^2)$ are form factors

The form of Kμν and (in the following, Wμν) follows from proton charge conservation and Lorentz invariance.

$$\frac{d\sigma}{d\Omega} = \left(\frac{1}{8\pi m_p}\right)^2 \left(\frac{E'}{E}\right)^2 \frac{(4\pi)^2\alpha^2}{4EE'\sin^4(\frac{\theta}{2})}\left(2K_1 \sin^2\theta/_2 + K_2 \cos^2\theta/_2\right)$$

$$= \frac{\alpha^2}{16 m_p^2 E^2}\left(\frac{E'}{E}\right)\frac{1}{\sin^4(\frac{\theta}{2})}\left(2K_1 \sin^2\frac{\theta}{2} + K_2 \cos^2\frac{\theta}{2}\right)$$

E, m form factor $\tau \equiv -\frac{q^2}{4m_p^2} > 0$

$K_1 = -q^2 G_M^2 = 4m_p^2 \tau G_M$

$K_2 = 4m_p^2\left[\frac{G_E^2 + \tau G_M^2}{1+\tau}\right]$

$$\frac{d\sigma}{d\Omega} = \frac{\alpha^2}{4E^2 \sin^4\theta/_2}\left(\frac{E'}{E}\right)\left(2\tau G_M^2 \sin^2\frac{\theta}{2} + \frac{G_E^2 + \tau G_M^2}{1+\tau}\cos^2\theta/_2\right)$$

proton recoil factor $\frac{E'}{E} = \frac{1}{1+\frac{2E}{m_p}\sin^2\frac{\theta}{2}}$

Rosenbluth Formula

You will show, in point charge limit $E'(\theta)$

$K_1 \to -q^2$

$K_2 \to 4m_p^2$

$G_E = G_M = 1$

<u>Inclusive, inelastic e-p scattering</u>

1987 Version of Griffiths; Halzen-Martin

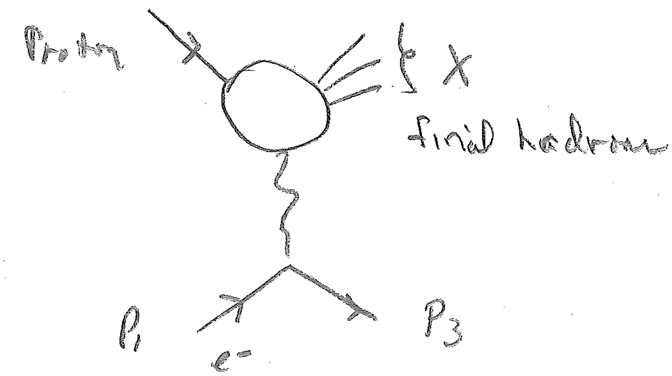

$$\langle |m|^2 \rangle = \frac{e^4}{q^4} L^{\mu\nu} K_{\mu\nu}$$

$$d\sigma = \frac{\langle |m|^2 \rangle}{\mathcal{F}} (2\pi)^4 \delta^4(\;) \frac{d^3p_3}{(2\pi)^3 2E_3} \prod_{\substack{\text{final} \\ \text{hadron}}} \frac{d^3p_i}{(2\pi)^3 2E_i}$$

$\mathcal{F} = 4\sqrt{(p_1 \cdot p_2)^2 - m_e m_p}$ flux factor

$$d\sigma = \frac{e^4}{q^4 \mathcal{F}} L^{\mu\nu} \frac{d^3p_3}{(2\pi)^3 2E_3} 4\pi m_p W_{\mu\nu}$$

$$4\pi m_p W_{\mu\nu} = \sum_{\substack{\text{final state} \\ X}} \int \prod_i \frac{d^3p_i}{(2\pi)^3 2E_i} K_{\mu\nu} (2\pi)^4 \delta^4(q + p_2 - \Sigma p_i)$$

↑ final hadrons in X

$W^{\mu\nu}$ takes the form $(P \equiv P_2)$

$$W^{\mu\nu} = W_1\left(-g^{\mu\nu} + \frac{q^\mu q^\nu}{q^2}\right) + \frac{W_2}{m_p^2}\left(p^\mu - \frac{q\cdot P}{q^2} q^\mu\right)\left(p^\nu - \frac{q\cdot P}{q^2} q^\nu\right)$$

W_1, W_2 functions of two independent kinematic variables

$$q^2 \quad \text{and} \quad X = \frac{-q^2}{2P\cdot q}$$

$$\text{or} \quad \nu = \frac{P\cdot q}{m_p}$$

Lab frame kinematics $(m_e \cong 0)$

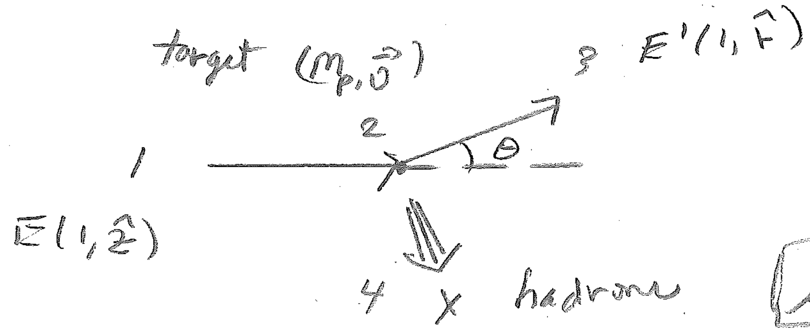

$\boxed{s \equiv \sin^2 \theta/2}$

$$-q^2 = 4EE's^2 \qquad X = \frac{2EE's^2}{m_p(E-E')}$$

$$\nu = E - E' \qquad \left\{ \frac{-q^2}{2X} = m_p \nu \right.$$

$$\frac{d\sigma}{dE'\,d\Omega} = \left(\frac{\alpha}{2Es^2}\right)^2 \left[2W_1 s^2 + W_2 \cos^2 \theta/2\right]$$

$$W_1(q^2, x) \qquad W_2(q^2, x)$$

Relation to elastic scattering

Change variables from E' to x

$$x = \frac{2Es^2}{m_p}\left(\frac{E'}{E-E'}\right) = \frac{2E^2s^2}{m_p}\left(\frac{1}{E'}-\frac{1}{E}\right)^{-1}$$

$$x\left(\frac{1}{E'}-\frac{1}{E}\right) = \frac{2E^2s^2}{m_p}$$

during E' integral with θ fixed, $\frac{2E^2s^2}{m_p} = \text{const}$

take derivative w.r.t. x

$$\left(\frac{1}{E'}-\frac{1}{E}\right) + x\left(\frac{-1}{E'^2}\right)\frac{dE'}{dx} = 0$$

$$\frac{dE'}{dx} = \frac{E'^2}{x}\left(\frac{1}{E'}-\frac{1}{E}\right) = \frac{E'^2}{x}\left(\frac{E-E'}{E'E}\right) = \frac{E'}{E}\frac{1}{x}(E-E')$$

with
$$\left.\begin{aligned} -q^2 &= 4EE's^2 \\ x &= \frac{2EE's^2}{m_p(E-E')} \end{aligned}\right\} \quad E-E' = \frac{-q^2}{2x m_p}$$

$$\frac{dE'}{dx} = \frac{-q^2}{2m_p x^2}\left(\frac{E'}{E}\right)$$

then if we let
$$\boxed{W_i(q^2,x) = \frac{K_i(q^2)}{2m_p(-q^2)}\,\delta(x-1)}$$

$$A \equiv \frac{\alpha}{2Es^2}$$

$$\frac{d\sigma}{d\Omega} = \int_0^E dE'\, A\left[2W_1 s^2 + W_2 \cos^2\theta/2\right]$$

$$\frac{d\sigma}{d\Omega} = \int_0^\infty dx \; A^2 \left(\frac{-q^2}{2m_p x^2}\right)\left(\frac{E'}{E}\right) \delta(x-1) \frac{1}{2m_p}\left(\frac{1}{-q^2}\right) [\;]$$

$$[\;] = 2K_1 s^2 + k_2 \cos^2 \theta/2$$

$$\frac{d\sigma}{d\Omega} = \frac{A^2}{4m_p^2}\left(\frac{E'}{E}\right)[\;]$$

$$\frac{A^2}{4m_p^2} = \left(\frac{\alpha}{2Es^2}\right)^2 \frac{1}{4m_p^2} = \left(\frac{\alpha}{4m_p E s^2}\right)^2$$

we recover elastic scattering cross section with

$$\frac{E'}{E} = \frac{1}{1 + \frac{2E}{m_p} s^2} \quad \text{constraint.}$$

Parton Model

Bjorken (BJ) scaling – at high energy

$W_i(q^2, x) \to$ function of x only

$$m_p W_1(q^2, x) \to F_1^{BJ}(x)$$

$$\frac{-q^2}{2 m_p x} W_2 \to F_2^{BJ}(x)$$

$-q^2 = 4EE'\theta^2$ and $q \cdot p = m_p(E-E')$ are large but ratio

$$x \equiv \frac{-q^2}{2 q \cdot p} = \frac{-q^2}{2 m_p \nu} \qquad \nu \equiv E - E'$$

You can show $0 \le x \le 1$

So $\nu W_2(q^2, x) = F_2^{BJ}(x)$

from Halzen-Martin

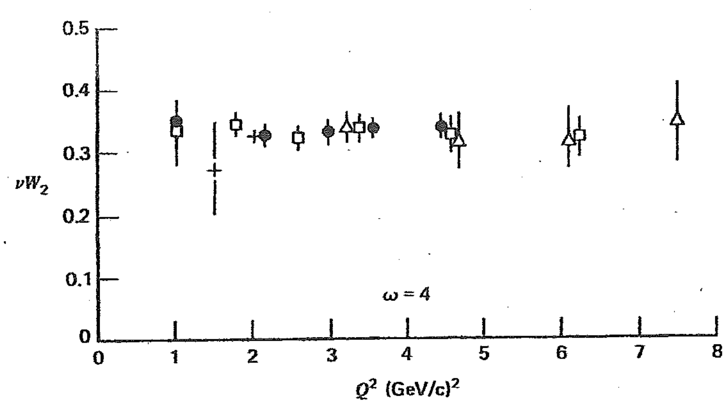

Fig. 9.2 The structure function νW_2 determined by electron–proton scattering as a function of Q^2 for $\omega = 4$. Data are from the Stanford Linear Accelerator.

$$x = \frac{1}{\omega} = \frac{1}{4}$$

<u>Following Halzen, Martin</u> # 9-9

At large $Q^2 \equiv -q^2$, virtual γ^* is resolving quark inside the proton

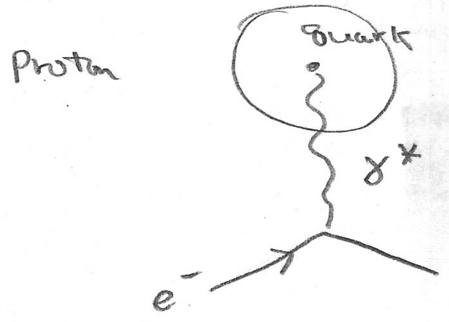

de Broglie wavelength

$$\frac{hc}{Q} = \frac{1240 \text{ MeV}}{1000 \text{ MeV}} \approx 1 \text{ fm}$$

recall, ep inelastic $\rightarrow$ ep elastic with

$$W_i(Q^2, x) = \frac{k_i(Q^2)}{2m\, Q^2}\,\delta(1-x)$$

point-like (e.g. eμ scattering) recovered with $(m = m_p)$

$$k_1 = Q^2 \; ; \; k_2 = 4m^2$$

$$W_1^{\text{point}} = \frac{1}{2m}\delta(1-x) \; ; \; W_2^{\text{point}} = \frac{2m}{Q^2}\delta(1-x)$$

<u>Quarks inside proton.</u>

Viewed in proton "infinite momentum frame" interaction between quarks is slowed down by time dilation, quarks are $\simeq$ free. e-p scattering is <u>incoherent</u> sum of quark scattering:

Each quark charge q_i with <u>momentum fraction z</u> of proton.

Proton	quark
E	zE
P_L	zP_L
$P_T = 0$	0
M	$m_q = (z^2E^2 - z^2P_L^2) = zM$

? variable mass ?

<u>but</u>, in infinite momentum frame, $m_q \cong zM \cong 0$.

Resolving the Blob

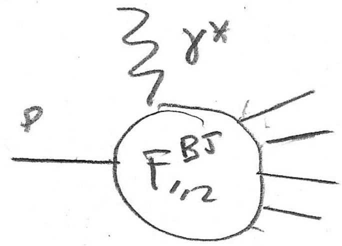

$$= \sum_{\text{quarks}} q_i^2 \int dz \Big[$$

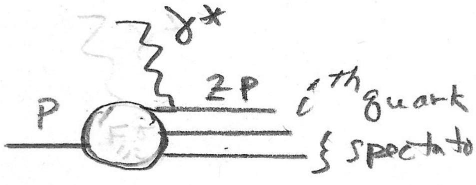

$$\Big]$$

$$\left[f_i(z)\, F^q_{12}(z) \right]$$

$F^{BJ}_{1,2}$ Bjorken scaling functions

$f_i(z)$ probability for i^{th} quark to have momentum fraction z

$$\sum_i \int dz\, z\, f_i(z) = 1 \qquad \text{sum to total proton momentum}$$

$F^q_{1,2}(z)$ single quark structure functions.

look carefully at W_2^{Point}:

$$m_i = zm$$

$$W_2^q = \frac{2m_i}{Q^2}\,\delta(1-x_i) \qquad x_i = \frac{Q^2}{2q\cdot P_i} = \frac{Q^2}{2q\cdot Pz} = \frac{x}{z}$$

$$= \frac{2zM}{Q^2}\,\delta\left(1-\frac{x}{z}\right) = \frac{z}{\nu}\,\delta(x-z) \qquad \boxed{\nu = \frac{Q^2}{2xm}}$$

$$\nu W_2^q = z\,\delta(x-z) = F_2^q$$

$$2m W_1^q = \frac{1}{2x}\,\delta\left(1-\frac{x}{z}\right) = \frac{1}{2}\frac{z}{x}\,\delta(x-z) = \frac{1}{2}\,\delta(x-z)$$

$$F_2^{BJ}(x) = \sum_i q_i^2 \int dz\, f_i(z)\, F_2^q = x \sum q_i^2 f_i(x)$$

$$F_1^{BJ}(x) = \sum_i q_i^2 \int dz\, f_i(z)\, F_1^q = \frac{1}{2}\sum q_i^2 f_i(x)$$

$$\boxed{F_2^{BJ} = 2x F_1^{BJ}}$$ experimentally verified

In terms of $F_{1,2}^{BJ}$ $\quad \left(A = \frac{\alpha}{2E s^2} \right)$

$$\frac{d\sigma}{dE' d\Omega} = A^2 \left[2W_1 s^2 + W_2 \cos^2\theta/2 \right]$$

$$W_1 = \frac{1}{m} F_1^{BJ} \; ; \; W_2 = \frac{2mx}{Q^2} F_2^{BJ} = \frac{2x}{\nu} F_1^{BJ}$$

$$\frac{d\sigma}{dE' d\Omega} = \left(\frac{\alpha}{2E s^2} \right)^2 \left(\frac{2}{m} \right) F_1^{BJ}(x) \left[s^2 + \frac{xm}{\nu} \cos^2\theta/2 \right]$$

$$x = \frac{2EE' s^2}{m\nu} \qquad \frac{xm}{\nu} = \frac{2EE' s^2}{\nu}$$

$$\frac{d\sigma}{dE' d\Omega} = \frac{\alpha^2}{2E^2 m} \frac{F_1^{BJ}(x)}{s^2} \left[1 + \left(\frac{2EE'}{E - E'} \right) \cos^2 \frac{\theta}{2} \right]$$

Structure functions

Proton contains valence and sea quarks

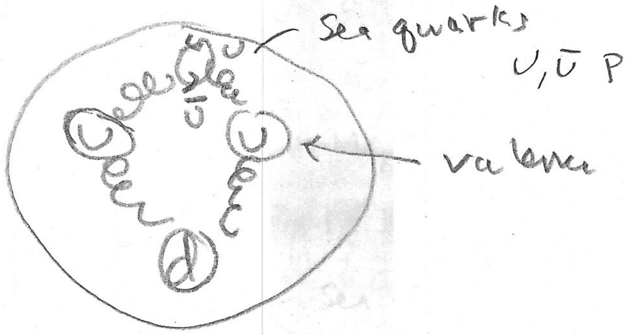

$f_u(x) \equiv u(x)$ valence + sea $\bar{u}(x)$ sea only

$$F_2^{\text{BJ Proton}}(x) = \frac{4}{9}\,x\left[u(x)+\bar{u}(x)\right] + \frac{1}{9}\,x\left[d(x)+\bar{d}(x)+s(x)+\bar{s}(x)\right]$$

with sum rule

$$\int_0^1 dx\; x\left[u+\bar{u}+d+\bar{d}+s+\bar{s}\right] \stackrel{?}{=} 1$$

$$\int_0^1 dx\left[u-\bar{u}\right] = 2$$

$$\int_0^1 dx\left[d-\bar{d}\right] = 1$$

$$\int_0^1 dx\left[s-\bar{s}\right] = 0$$

experimentally we find $\int_0^1 dx\; x\left[u+\bar{u}+d+\bar{d}+s+\bar{s}\right] \simeq \frac{1}{2}$

$e-p$, $\mu-p$, $\nu-p$

the rest is glue!

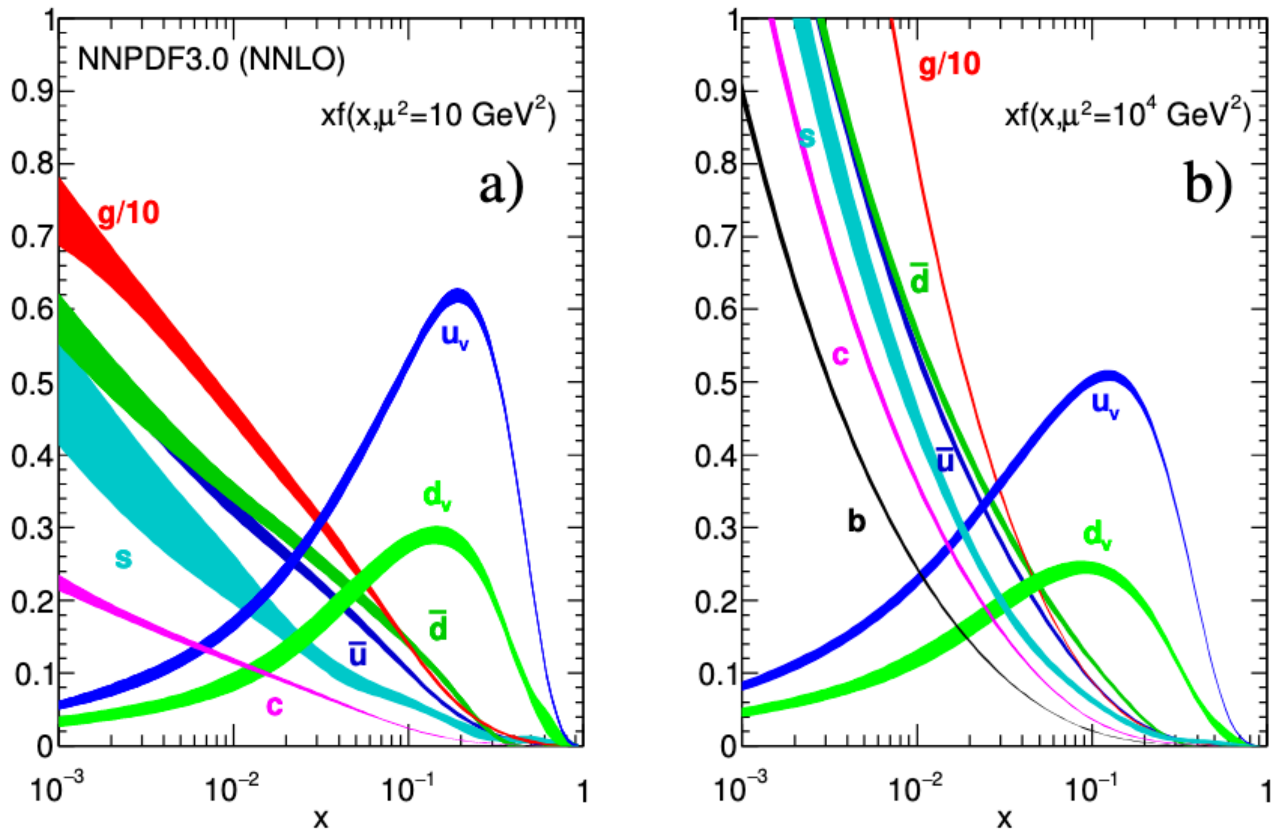

from PDG. note more glue at higher scale μ

γ∗->q
γ∗->qg
QCD corrections

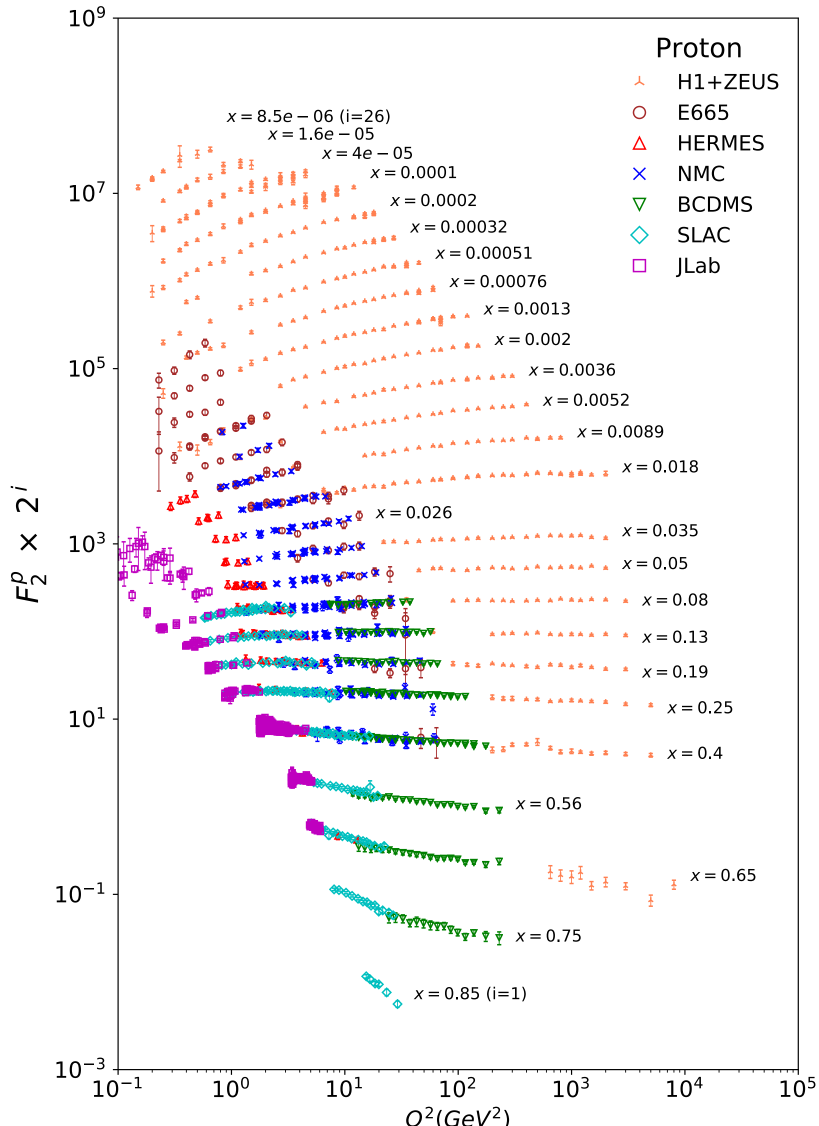

QCD corrections give Q^2 dependence especially at low x

Figure 18.8: The proton structure function F_2^p measured in electromagnetic scattering of electrons and positrons on protons, and for electrons/positrons (SLAC,HERMES,JLAB) and muons (BCDMS, E665, NMC) on a fixed target. Statistical and systematic errors added in quadrature are shown. The H1+ZEUS combined values are obtained from the measured reduced cross section and converted to F_2^p with a HERA-PDF NLO fit, for all measured points where the predicted ratio of F_2^p to reduced cross-section was within 10% of unity. The data are plotted as a function of Q^2 in bins of fixed x. Some points have been slightly offset in Q^2 for clarity. The H1+ZEUS combined binning in x is used in this plot; all other data are rebinned to the x values of these data. For the purpose of plotting, F_2^p has been multiplied by 2^{i_x}, where i_x is the number of the x bin, ranging from $i_x = 1$ ($x = 0.85$) to $i_x = 26$ ($x = 0.0000085$). Only data with $W^2 > 3.5$ GeV^2 is included. Plot from CJ collaboration (Shujie Li – private communication). References: **H1 and ZEUS**—H. Abramowicz *et al.*, Eur. Phys. J. **C75**, 580 (2015) (for both data and HERAPDF parameterization); **BCDMS**—A.C. Benvenuti *et al.*, Phys. Lett. **B223**, 485 (1989) (as given in [187]) **E665**—M.R. Adams *et al.*, Phys. Rev. **D54**, 3006 (1996); **NMC**—M. Arneodo *et al.*, Nucl. Phys. **B483**, 3 (1997); **SLAC**—L.W. Whitlow *et al.*, Phys. Lett. **B282**, 475 (1992); **HERMES**—A. Airapetian *et al.*, JHEP **1105**, 126 (2011);**JLAB**—Y. Liang *et al.*, Jefferson Lab Hall C E94-110 collaboration, nucl-ex/0410027, M.E. Christy *et al.*, Jefferson Lab Hall C E94-110 Collaboration, Phys. Rev. **C70**, 015206 (2004), S. Malace *et al.*, Jefferson Lab Hall C E00-116 Collaboration, Phys. Rev. **C80**, 035207 (2009), V. Tvaskis *et al.*, Jefferson Lab Hall C E99-118 Collaboration, Phys. Rev. **C81**, 055207 (2010), M. Osipenko *et al.*, Jefferson Lab Hall B CLAS6 Collaboration, Phys. Rev. **D67**, 092001 (2003).

property is related to the assumption that the transverse momentum of the partons in the infinite-momentum frame of the proton is small. In QCD, however, the radiation of hard gluons from the quarks violates this assumption, leading to logarithmic scaling violations, which are particularly large at small x, see Fig. 18.2. The radiation of gluons produces the evolution of the structure functions. As Q^2 increases, more and more gluons are radiated, which in turn split into $q\overline{q}$ pairs. This process leads both to the softening of the initial quark momentum distributions and to the growth of the gluon density and the $q\overline{q}$ sea as x decreases.

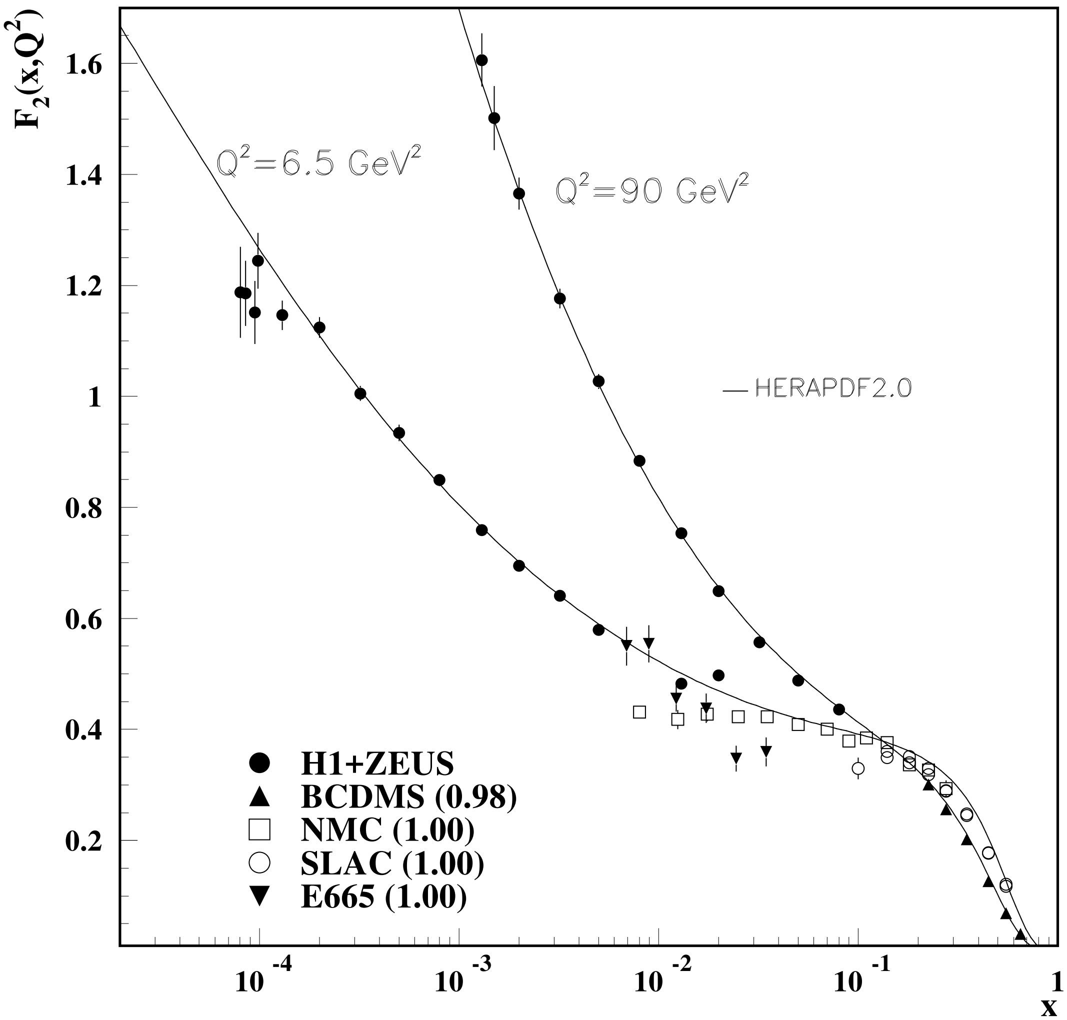

Figure 18.2: The proton structure function F_2^p given at two Q^2 values (6.5 GeV^2 and 90 GeV^2), which exhibit scaling at the 'pivot' point $x \sim 0.14$. See the captions in Fig. 18.8 and Fig. 18.10 for the references of the data. The various data sets have been renormalized by the factors shown in brackets in the key to the plot, which were globally determined in a previous HERAPDF analysis [13]. The curves were obtained using the PDFs from the HERAPDF analysis [14]. In practice, data for the reduced cross section, $F_2(x,Q^2) - (y^2/Y_+)F_L(x,Q^2)$, were fitted, rather than F_2 and F_L separately. The agreement between data and theory at low Q^2 and x can be improved by a positive higher-twist correction to $F_L(x,Q^2)$ [15,16] (see Fig. 8 of Ref. [16]), or small-x resummation [17,18].

In QCD, the above processes are described in terms of scale-dependent parton distributions $f_a(x,\mu^2)$, where $a = g$ or q and, typically, μ is the scale of the probe Q. For parton distributions x

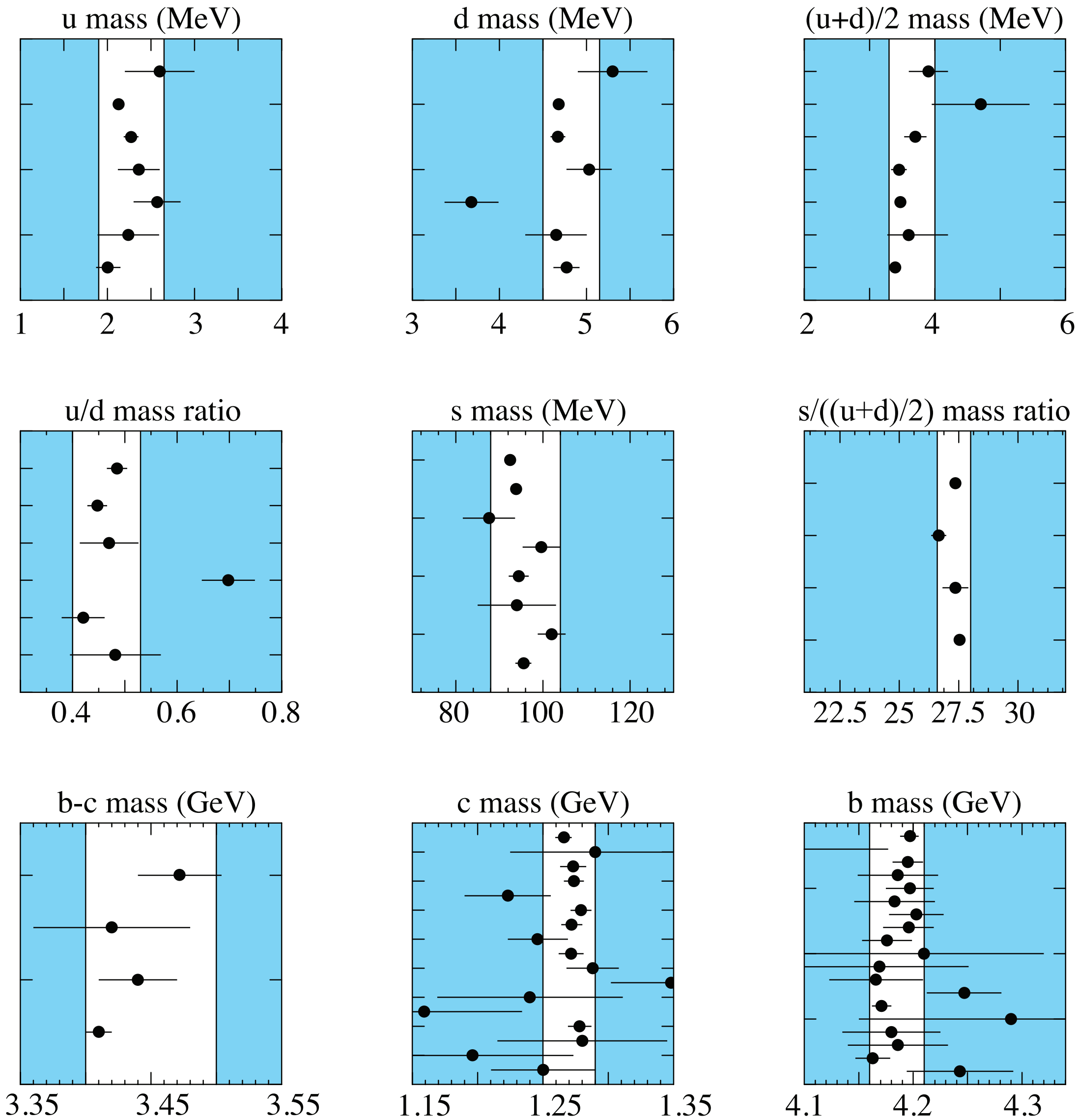

Figure 59.3: The values of each quark mass parameter taken from the Data Listings. The points are in chronological order with the more recent measurements at the top. The shaded regions indicate values excluded by our evaluations; some regions were determined in part through examination of Fig. 59.2.

References:

1. See the review of QCD in this volume..
2. A.V. Manohar and H. Georgi, Nucl. Phys. **B234**, 189 (1984).
3. K.G. Chetyrkin, Phys. Lett. **B404**, 161 (1997).
4. J.A.M. Vermaseren, S.A. Larin, and T. van Ritbergen, Phys. Lett. **B405**, 327 (1997).
5. K.G. Chetyrkin, B.A. Kniehl, and M. Steinhauser, Nucl. Phys. **B510**, 61 (1998).

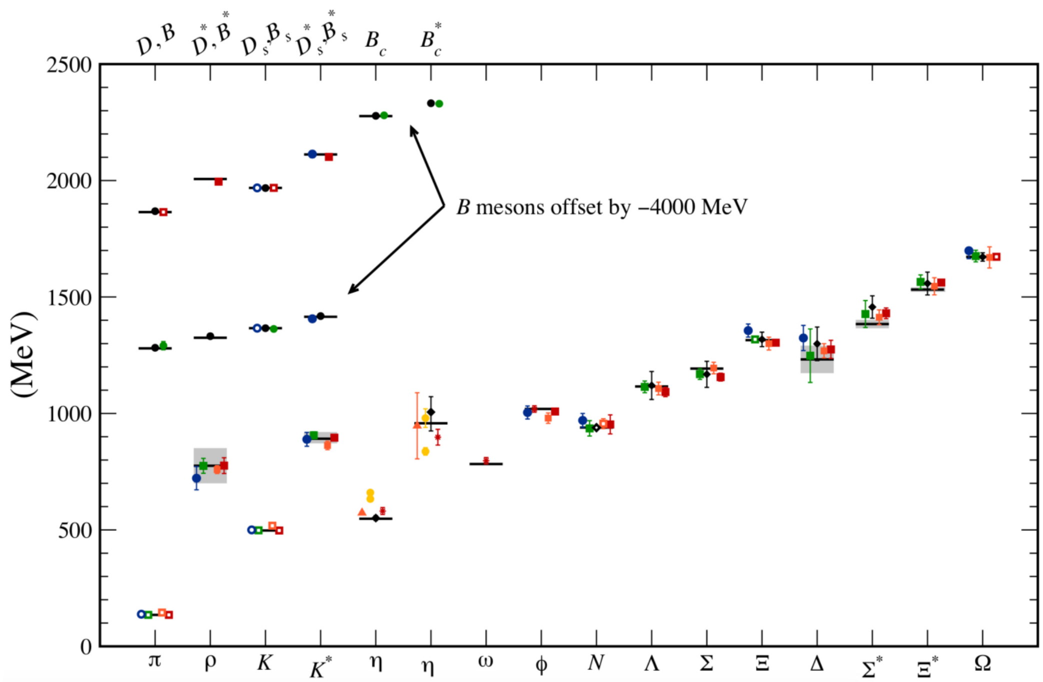

Figure 15.7: Hadron spectrum from lattice QCD. Comprehensive results for mesons and baryons are from MILC [65,66], P CS-CS [67], BMW [68], QCDSF [69], and ETM [70]. Results for η and η' are from RBC & UKQCD [10], Hadron Spectrum [71] (also the only ω mass), UKQCD [72], and Michael, Ottnad, and Urbach [73]. Results for heavy-light hadrons from Fermilab-MILC [74], HPQCD [75,76], and Mohler and Woloshyn [77]. Circles, squares, diamonds, and triangles stand for staggered, Wilson, twisted-mass Wilson, and chiral sea quarks, respectively. sterisks represent anisotropic lattices. Open symbols denote the masses used to fix parameters. Filled symbols (and asterisks) denote results. Red, orange, yellow, green, and blue stand for increasing numbers of ensembles (i.e., lattice spacing and sea quark mass) Black symbols stand for results with 2+1+1 flavors of sea quarks. Horizontal bars (gray boxes) denote experimentally measured masses (widths). b-flavored meson masses are offset by 4000 MeV.

provided by S. Meinel [81]. The state recently announced by LHCb [36] is also shown. Note that the lattice calculations for the mass of this state were predictions, not postdictions.

Recall that lattice calculations take operators which are interpolating fields with quantum numbers appropriate to the desired states, compute correlation functions of these operators, and fit the correlation functions to functional forms parametrized by a set of masses and matrix elements. s we move away from hadrons which can be created by the simplest quark model operators (appropriate to the lightest meson and baryon multiplets) we encounter a host of new problems: either no good interpolating fields, or too many possible interpolating fields, and many states with the same quantum numbers. Techniques for dealing with these interrelated problems vary from collaboration to collaboration, but all share common features: typically, correlation functions from many different interpolating fields are used, and the signal is extracted in what amounts to a variational calculation using the chosen operator basis. In addition to mass spectra, wave function information can be garnered from the form of the best variational wave function. Of course, the same problems which are present in the spectroscopy of the lightest hadrons (the need to extrapolate to infinite volume, physical values of the light quark masses, and zero lattice spacing) are also present. We briefly touch on three different kinds of hadrons: excited states of mesons (including hybrids),

$e^+e^- \longrightarrow$ hadrons

$e^+e^- \rightarrow \mu^+\mu^-$ $\quad \frac{d\sigma}{d\Omega} = \frac{\alpha^2}{4s}\left(1 + \cos^2\theta\right)$ $\quad$ high energy limit

$s = (2E_b)^2$ $\quad E_b$ beam energy of each e^-, e^+

angular distribution can be understood in terms of angular momentum conservation

$\overset{\vec{S}}{\Rightarrow}$ $\longrightarrow \vec{p}$ $\quad$ helicity +1 $\quad$ right handed

$\overset{\vec{S}}{\Leftarrow}$ $\longrightarrow \vec{p}$ $\quad$ helicity −1 $\quad$ left handed

at high energy ($m = 0$) helicity is conserved by EM interaction

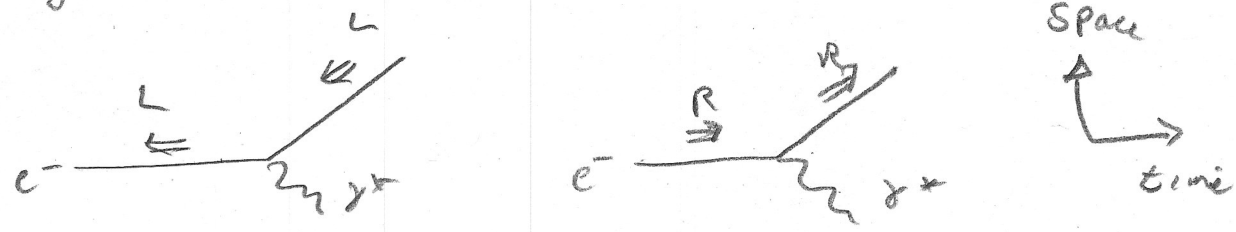

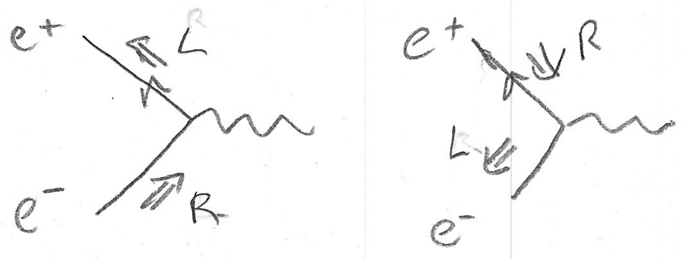

e+ is e⁻ moving backward in time

#9-14

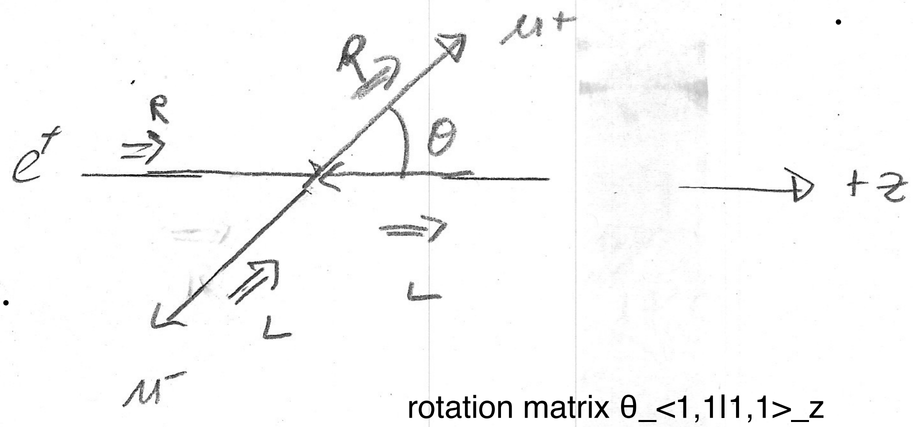

rotation matrix θ_<1,1l1,1>_z

$$A(LR \to LR) \propto d^1_{1,1}(\theta) = \frac{1+\cos\theta}{2} = A(RL \to RL)$$

$$A(LR \to RL) = \frac{1-\cos\theta}{2} = A(RL \to LR)$$

squaring and summing gives

$$\frac{d\sigma}{d\Omega} \propto \frac{1}{2}(1+\cos^2\theta)$$

Jet axis in $e^+e^- \to$ hadrons (2 jets) gives this angular distribution: <u>spin-$\frac{1}{2}$ quarks</u>

evidence for spin $\frac{1}{2}$ quarks

$$\frac{d\sigma}{d\Omega} \propto (1+\cos^2\theta)$$

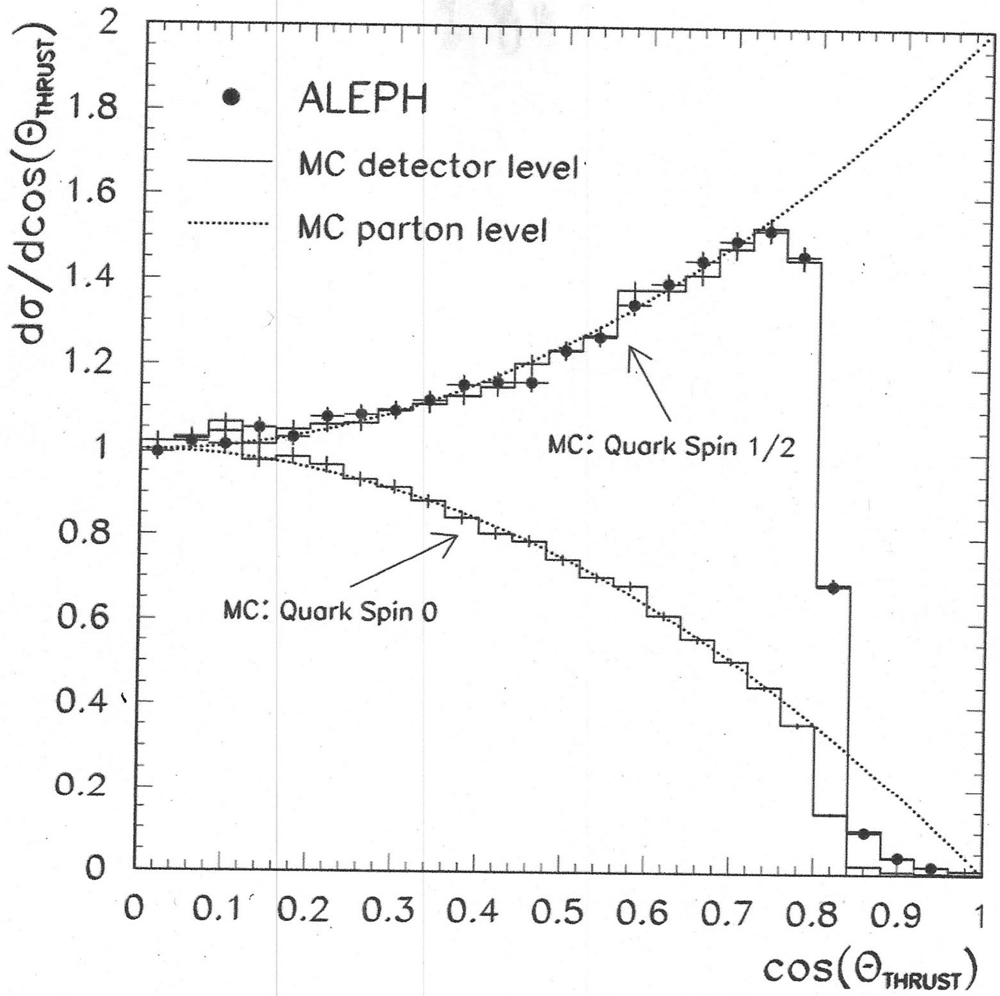

9-16

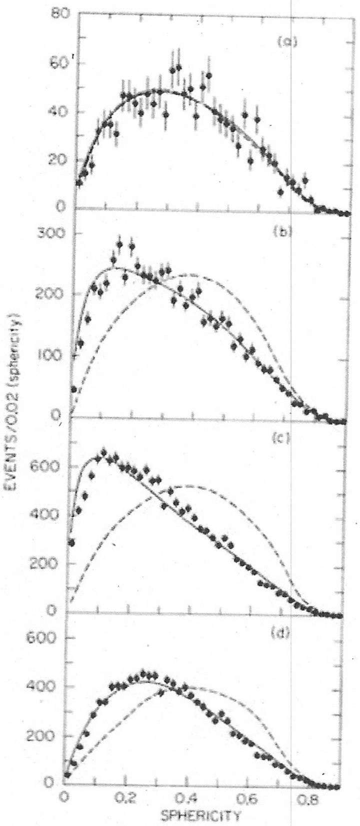

FIG. 2. Observed sphericity distributions for data, jet model with $\langle p_\perp \rangle = 315$ MeV/c (solid curves), and phase-space model (dashed curves) for (a) $E_{c.m.} = 3.0$ GeV; (b) $E_{c.m.} = 6.2$ GeV; (c) $E_{c.m.} = 7.4$ GeV; and (d) $E_{c.m.} = 7.4$ GeV, events with largest $x < 0.4$. The distributions for the Monte Carlo models are normalized to the number of events in the data.

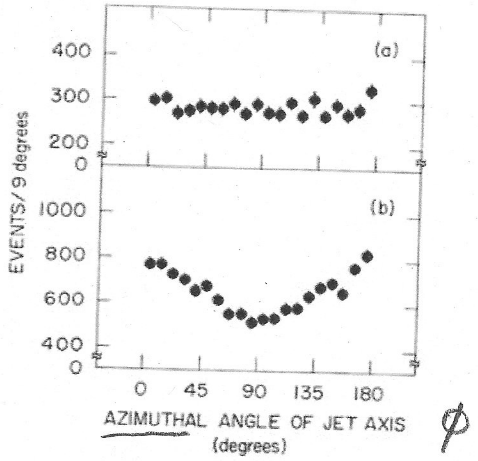

FIG. 3. Observed distributions of jet-axis azimuthal angles from the plane of the storage ring for jet axes with $|\cos\theta| \leq 0.6$ for (a) $E_{c.m.} = 6.2$ GeV and (b) $E_{c.m.} = 7.4$ GeV.

the jet model [Figs. 2(b) and 2(c)]. At the highest two energies, the PS model poorly reproduces the single-particle momentum spectra, having fewer particles with $x > 0.4$ ($x = 2p/E_{c.m.}$ and p is the particle momentum) than the data.[8] The jet-model x distributions are in better agreement. For $x < 0.4$ the x distributions for both models agree with the data. Therefore, we show in Fig. 2(d) the S distributions at 7.4 GeV for those events in which *no* particle has $x > 0.4$. The jet model is still preferred.

At $E_{c.m.} = 7.4$ GeV the electron and positron beams in the SPEAR ring are transversely polarized, and the hadron inclusive distributions show an azimuthal asymmetry.[9] The φ distributions of the jet axis for jet axes with $|\cos\theta| \leq 0.6$ are shown in Fig. 3 for 6.2 and 7.4 GeV.[10] At 6.2 GeV, the beams are unpolarized[9] and the φ distribution is flat, as expected. At 7.4 GeV, the φ distribution of the jet axis shows an asymmetry with maxima and minima at the same values of φ as for $e^+e^- \to \mu^+\mu^-$.

The φ distribution shown in Fig. 3(b) and the value for P^2 (0.47 ± 0.05) measured simultaneously by the reaction[9] $e^+e^- \to \mu^+\mu^-$ were used to determine the parameter α of Eq. (4). The value obtained for the *observed* jet axis is $\alpha = 0.45 \pm 0.07$. This observed value of α will be less than the true value which describes the production of the jets because of the incomplete acceptance of the detector, the loss of neutral particles, and our method of reconstructing the jet axis. We have used the jet-model Monte Carlo simulation to estimate the ratio of observed to produced values of α and find this ratio to be 0.58 at 74 GeV. Thus the value of α describing the *produced* jet-axis angular distribution is $\alpha = 0.78 \pm 0.12$ at $E_{c.m.} = 7.4$ GeV. The error in α is statistical only; we estimate that the systematic errors in the observed α can be neglected. However, we have not studied the model dependence of the correction factor relating observed to produced values of α.

The sphericity and the value of α as determined above are properties of whole events. The simple jet model used for the sphericity analysis can also be used to predict the single-particle inclusive angular distributions for all values of the secondary particle momentum. In Fig.

for e^+e^- polarized $\perp$ beam,

$$\frac{d\sigma}{d\Omega} \propto 1 + \alpha \cos^2\theta + P^2 \alpha \sin^2\theta \cos 2\phi$$

P polarization $\alpha = 1$ for spin $\frac{1}{2}$, -1 spin 0